#24-016
2024 AFS Proceedings ©American Foundry Society

Influence of Niobium on the Microstructure of Hypereutectic Gray Cast Iron

G. Alonso
AZTERLAN, Basque Research and Technology Alliance (BRTA), Durango, Spain

I. Asenjo
AZTERLAN, Basque Research and Technology Alliance (BRTA), Durango, Spain

D.M. Stefanescu
The Ohio State University, Columbus, OH and The University of Alabama, Tuscaloosa, AL

B. Bravo
AZTERLAN, Basque Research and Technology Alliance (BRTA), Durango, Spain

R. Suárez
AZTERLAN, Basque Research and Technology Alliance (BRTA), Durango, Spain

ABSTRACT

The final properties of gray cast iron depend on graphite morphology. Additions of certain trace elements can improve or degrade these properties at constant carbon level. The goal of this research was to investigate the effect of different levels of niobium on the microstructure and nucleation propensity of hypereutectic gray cast irons. Cooling curves were recorded, and metallographic analysis was conducted, on thermal analysis (TA) inoculated cups. It was found that niobium additions significantly alter the solidification process, modifying the morphology, type and size of graphite, the number of eutectic cells and the pearlite spacing. These effects are more evident as the content of niobium increases. Early precipitation and growth of kish graphite (type C graphite) seems to be reduced. Mn sulfides nucleating on complex oxides were detected as the main nuclei through a scanning electron microscopy (SEM) study. The formation of NbTi particles is directly related to the Nb content.

Keywords: gray iron, graphite morphology, nucleation, niobium, kish graphite, mechanical properties

INTRODUCTION

Lamellar graphite cast iron is widely used in industry. Properties such as a high compression strength and thermal conductivity, an excellent ability to isolate vibrations and fill molds, a better machinability than other cast irons and its relatively low cost, converts this type of iron into an ideal material for the automotive industry. The final properties of gray cast iron are controlled by the graphite morphology and the volume fraction. The presence of standard alloying elements such as Nb, Mn, Ti, V, Cr**,** Sn, Cu or Mo alters the shape of the graphite and the metallic matrix, modifying mechanical properties.

Manganese promotes the pearlitic microstructure formation, increasing mechanical strength and toughness[1] participating also actively in the nucleation process of graphite forming (Mn,X)S compounds.[2] Titanium reacts with nitrogen present in cast irons, forming stable nitrides that, in addition to modifying the graphite flake length,[3] behave as excellent nucleation sites for lamellar graphite.[4,5] Vanadium is a strong carbide-forming element whose carbides are harder than those formed by titanium. Azzoug et al.[6] observed that additions of vanadium of 1%, 3% and 5% had a significant impact on the solidification process with the creation of new sites of nucleation but also, with a relevant drop in yield strength and tensile strength as the vanadium content increases. Additions of chromium modifies the solidification system with the formation of chromium-iron complex carbides, which lead to an improvement in hardness.[7,8]

Kus and Akgul[9] revealed that very little amounts of tin (Sn) can change the matrix structure and the morphology of graphite. The effect of copper was studied by Bates,[10] who observed that additions up to about 0.5% increased the yield strength and tensile strength, promoting pearlitic structure. According to Chen et al.,[11] increasing the Mo content from 0.03% to 0.078% improved the tensile strength around 100 MPa while the graphite length became shorter from 400 μm to 288 μm.

Presence of other trace elements like boron or lead, is usually linked to harmful effects. Boron seems to promote the formation of type B and type D graphite.[12-14] The presence of trace amounts of lead decrease both hardness and tensile strength because of the formation of undesirable mesh, Widmänstatten and spiky graphite.[15,16]

The role of niobium has been analyzed in depth by multitude of researchers during the last years. Decevely and Yakut[17] produced experimental cast iron alloys consisting of 3.65%C and 0.019, 0.151, 0.431 and 0.646% niobium. They noted a linear increase in the hardness and tensile strength when different amounts of Nb were added, obtaining the maximum for 0.646%Nb (Figure 1a). Several NbC phases, whose number grew as the niobium content increases, were also found.

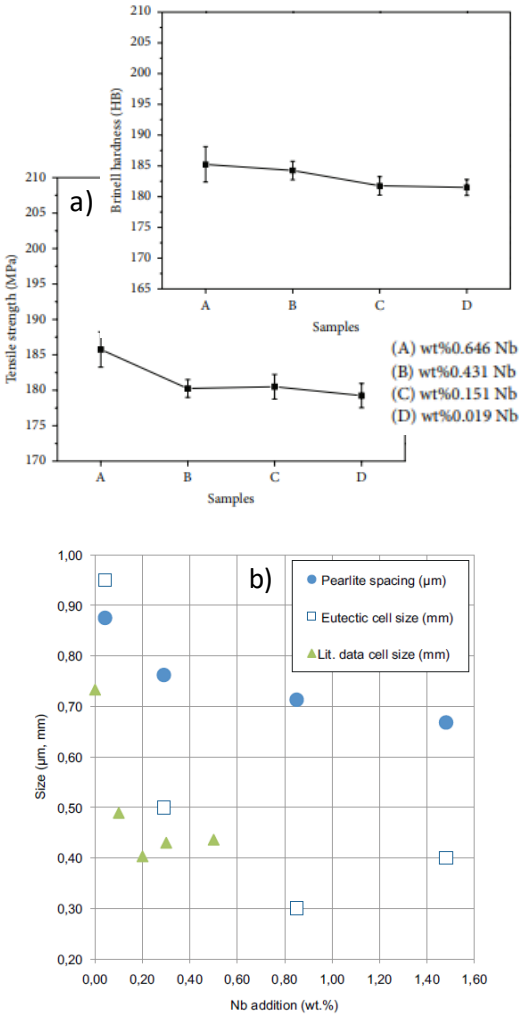

Figure 1. Effect of Nb addition: a) on tensile strength and hardness,[1] b) on microstructural refinement of eutectic cells and pearlite spacing.[2]

Mohrbacher et al.[18] found for irons with 3.82%C and 2.05%Si, that additions up to 0.2%Nb, refined significantly the morphology of graphite and the eutectic cells, reducing also the pearlite lamellar spacing. The effect is weaker from that level of Nb (Figure 1b). Formation of NbC precipitates merging in different shapes were observed for contents of 0.29%Nb and higher. Some of them seem to act as heterogeneous nucleation sites for graphite in the eutectic reaction. Zhou et al.[19] found that the 1.48%Nb addition to gray cast irons could increase hardness and wear resistance significantly due to the massive presence of large-sized NbC phases. Maximum tensile strength (300MPa) and mechanical fatigue properties were obtained for niobium contents of 0.20% and 0.16% respectively, in experimental trials carried out by Pan et al.[20]

The present investigation was designed to study the influence of niobium on the microstructure and the potential nucleation for hypereutectic gray cast irons. A series of thermal analysis cups with different contents of Nb were poured. Some plates were also obtained to analyze the mechanical properties. Samples were inoculated with an inoculant rich in Zr and Mn. Advanced SEM techniques were used for the identification of the possible nuclei.

DESIGN OF EXPERIMENTS

MELTING AND CASTING

Four heats with similar carbon equivalent (Ceq≈4.5) but different Nb contents (0.0.14, 0.30 and 0.48 mass%) were produced in a 100 kg medium frequency induction furnace (250Hz, 100Kw). The charge of each heat consisted of 63kg of ductile iron returns, 27kg of high purity iron and 200g of pyrite (50%Fe, 50%S). Predetermined amounts of a commercial graphite (98.9% C, 0.03% S) and of FeSi75 alloy (74.6% Si, 0.3% Ca, 0.7%Al) were also added to the metallic charges. Different quantities of pure Nb (99.8%) were introduced directly into the furnace. After superheating to 1500C (2732F), the iron was transferred into the pouring ladle. The chemical compositions of the experimental heats are presented in Table 1. In addition to the elements listed in the table, the alloys contained less than 0.010%Mo, Mg and Al, and less than 0.005%Sn. For each heat, 3 thermal analysis (TA) cups were poured, two of them inoculated. Inoculation was made directly in the cups through the addition of 0.2% of a commercial inoculant, ZrMn (62.6% Si, 6.77% Zr, 5.96% Mn, 1.79% Ca, 1.01% Al).

Two TA cups (one inoculated and one not) were used to record the cooling curves. The third cup (inoculated) was quenching in water after 20 seconds, in order to study the possible nuclei for graphite. In total, 12 standard TA cups were poured from the melts. Two plates of 150x50mm with two different thickness (10 and 40mm) were cast from each heat (8 plates in total) in order to evaluate the mechanical properties (hardness and tensile strength). All were also inoculated with 0,15%ZrMn inoculant.

Table 1. Chemical Composition (mass%) of Experimental Cast Irons

C	Si	CE	Mn	P	S	Cr	Cu	Ti	Nb
3.86	2.05	4.54	0.29	0.020	0.10	0.078	0.088	0.028	<0.005
3.88	1.97	4.54	0.31	0.022	0.11	0.10	0.11	0.027	0.14
3.86	1.93	4.50	0.30	0.023	0.11	0.11	0.12	0.026	0.30
3.87	1.90	4.50	0.29	0.021	0.10	0.12	0.11	0.025	0.48

CHARACTERIZATION

The temperature-time data were recorded and processed with the Thermolan® system to produce cooling curves (Figure 2). Information on eutectic maximum and minimum temperature, undercooling, recalescence, cooling rate (CR_{max}) and solidus and liquidus temperature were obtained from these curves. Significant differences were observed between the different TA cooling curves, depending on the content of niobium.

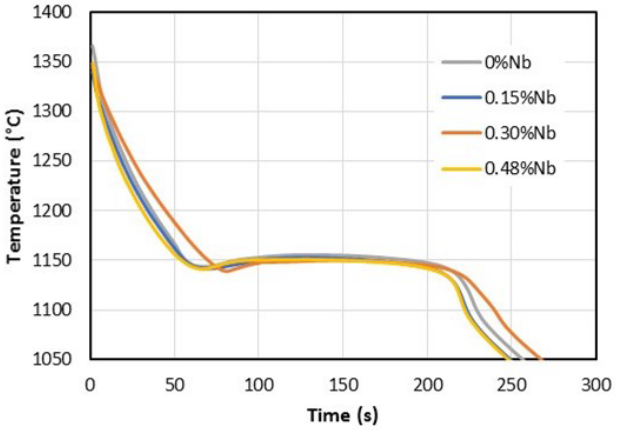

Figure 2. Cooling curves as a function of the niobium content.

After cooling to room temperature, the cups were sectioned and prepared (ground and polished) for metallographic examination. A total of 10 different fields were studied for each sample to analyze the morphology of lamellar graphite by optical microscopy. Image processing was performed by means of the Image J software to determine length, area, size, type of graphite and kish graphite/mm.^{2} To calculate the number of eutectic cells, samples were etched with a reactive consisted of 0.5gr picric acid, 1gr $CuCl_2$, 2ml HCl, 10ml H_2O and 100ml of ethanol. Three representative fields were acquired at 25x magnifications to evaluate them. For the evaluation of lamellar spacing of pearlite, samples were etched with Nital. Five fields were acquired at 1000x magnifications and several measurement lines were drawn perpendicularly to the pearlitic sheets for multiple assessments.

Two tensile test specimens of 10mm of diameter and M16 (according to UNE-EN 1561:2011) were machined from each plate to calculate tensile strength. A sample of 150 x 50mm with a thickness of 15 ±5mm was obtained of each plate for the Brinell hardness tests. Three measurements were done per sample according to UNE.-EN ISO 6506-1:2015.

To identify possible nucleation sites an Ultra PLUS Carl Zeiss SMT (0.8 mm resolution at 30 kV) in the STEM mode was used in combination with an X-Max 20 Oxford Instruments EDX detector with a resolution of 127 eV/ mm2. The most advanced SEM techniques such as spectrums, mappings and line scans, were applied to analyze the main elements present in the inclusions and to estimate the type of compounds which can act as nuclei for graphite.

RESULTS AND DISCUSSION

INFLUENCE OF Nb ON THE COOLING CURVES

The experimental results obtained from the cooling curves are summarized in Table 2. Relevant changes are produced in the solidification process because of the addition of niobium.

Table 2. Experimental Data from Cooling Curves.

Terminology: TL_A - liquidus arrest temperature; TE_{max}. – eutectic maximum temperature; TE_{min}. – eutectic minimum temperature; ΔT_{recal}. - recalescence; T_{sol}. – solidus minimum temperature; CR_{max} – maximum cooling rate at the end of solidification

%Nb	TL_A (ºC)	TE_{max} (ºC)	TE_{min} (ºC)	ΔT_{recal} (ºC)	Undercooling (ºC)	T_{sol} (ºC)	CR_{max} (ºC/s)
0	1151.3	1155.8	1144.0	11.8	17.5	1127.2	3.9
0.15	1145.8	1152.7	1141.4	11.3	19.7	1129.6	4.05
0.30	1142.9	1150.0	1139.1	10.9	21.9	1135.2	2.52
0.48	1142.0	1150.7	1141.2	9.5	19.7	1126.0	4.42

Both liquidus arrest temperature and recalescence decrease as the content of niobium of the melt increases, reaching the minimum for 0.48%Nb (1142.0ºC for T_{LA} and 9.5 for ΔT_{recal}) (Figure 3). In the case of TE_{min} and TE_{max} this assertion is true but only up to 0.30%Nb, value form which both parameters present a slight increase (Figure 3). However, note that for this particular sample, the cooling rate was much slower than for the other samples. Higher values of recalescence are related to a high amount of graphite precipitation in the early stage of eutectic solidification, so the addition of niobium appears to hinder the formation of graphite. As expected, an inverse relation was found between undercooling and eutectic minimum temperature, with a maximum of 21.9 for 0.30%Nb, where the undercooling is calculated by the Eqn.1.

Undercooling= Teut.theor. - TE_{min} **Eqn 1**

and Teut.theor. is defined by Eqn. 2:

Teut.theor. = 1154.02 + 4.86*%Cu – 5*%Mn – 2.60*%Ni + 4.246*%Si[21] **Eqn 2**

No clear correlation was observed for the solidus temperature and cooling rate.

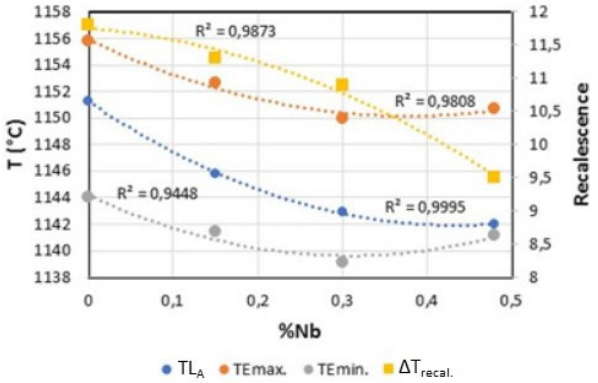

Figure 3. Evolution of the TL_A, TE_{min}, TE_{max} and recalescence in function of the content of Nb in the melt.

INFLUENCE OF Nb ON THE MICROSTRUCTURE

Significant variations on the microstructure were observed in function of the different contents of niobium in the base melt (Table 3).

Table 3. Experimental Results Listed for % Niobium Content

%Nb	Length Gr. (µm)	Area Gr. (µm²)	Type Gr.	Size Gr.	%Ferrite	Kish Gr./mm²	Eutectic cells/mm²	Pearlite spacing (µm)
0	75.1	10.8	85%A+10%C'+5%E	3-4	<2%	2.44	5.1	0.769
0.15	51.9	9.8	90%A+5%C'+5%E	4-5	<1%	0.6	5.1	0.634
0.30	49.0	9.7	95%A+5%D	5-6	<1%	1.37	8.3	0.604
0.48	46.6	8.8	95%A+5%D	5-6	<1%	0.94	12.3	0.550

The morphology of graphite is highly influenced by the presence of niobium. A clear tendency was found between the length and area of graphite, and the additions of niobium. Both parameters decreased as the %Nb increased (Figure 4). In the case of the length of graphite, this reduction is almost 40% (75.1µm for 0%Nb and 46.6µm for 0.48%Nb).

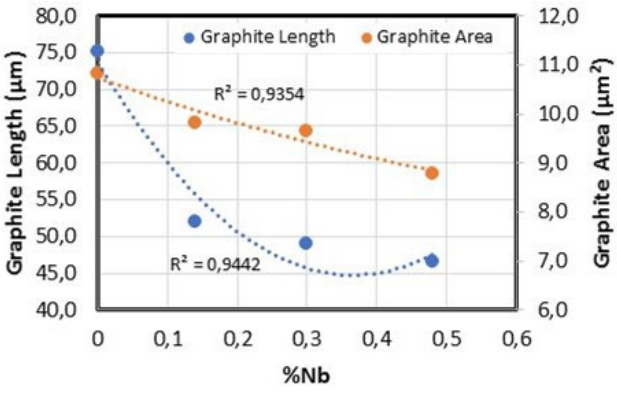

Figure 4. Evolution of the parameters of graphite in function of the content of Nb in the melt.

Nb produces shorter and thinner graphite, favoring the formation of smaller graphite (size 5-6 for 0.48%Nb versus 3-4 without Nb) (Figure 5). Nb seems to hinder the growth of graphite. Similar conclusions were drawn by Morhbacher and Zhai,[18] who estimated the finest graphite size for 0.85%Nb. Niobium does not modify the structure of the matrix, which is fully pearlitic in all cases, with only some traces of ferrite.

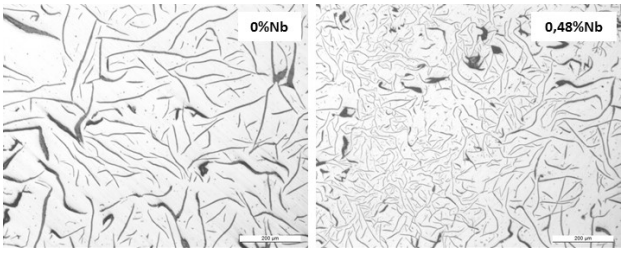

Figure 5. Changes in the morphology of graphite because of the presence of niobium.

Noticeable changes were also observed in the type of graphite generated. Nb appears to stimulate the formation of type A graphite. Low percentages of graphite type C' and E were detected for low content of niobium, disappearing from 0.30%Nb. This type C' graphite is also known as kish graphite. It is a proeutectic graphite precipitate that, many times, appears to form on the free surface of molten irons. It is characterized by a bigger size and a foliated dendritic structure with a substantial tilting and branching of the platelets (Figure 6a).[22,23] This kish graphite was also detected in quenched samples (Figure 6b). It seems to occur during the first moments of solidification and surrounding itself by a shell of austenite. The formation of this type of graphite is affected by the presence of niobium. The maximum amount of kish graphite was reached for no additions of Nb (Figure 6c). Significant reductions were produced with the content of niobium, reaching a minimum of 0.6 kish Gr/mm^2 for 0.15%Nb.

Figure 6. Presence of kish graphite on samples without niobium; a) deep etched SEM micrograph showing the branching of the kish graphite; b) quenched sample with a solid fraction of 0.35 calculated by the method described in Reference 24; c) thermal analysis cup, where the kish graphite was identified by red circles.

The effect of niobium content on the eutectic cell size is evident. Additions of 0.15%Nb does not alter the formation of eutectic cells. Contents of 0.3%Nb multiply their number by a factor of 1.7 (8.3 eutectic cell/mm^2). This effect is even more noticeable for 0.48%Nb addition, which multiplies by more than double the distribution density of eutectic cells (12.3 versus 5.1, for 0.48%Nb and 0%Nb respectively) (Figure 7a,b). The pattern followed by this parameter is just the opposite of that for the length of graphite; the number of eutectic cells increases as graphite becomes finer (Figure 7c). According to Pan et al.[20] the number of eutectic cells is equal to the number of graphite cores, which could explain the similar refining trend of graphite and eutectic cells.

The presence of niobium progressively decreases the pearlite interlamellar spacing. This effect is especially pronounced for low additions of niobium (0.15%Nb) (Figure 8). The finest pearlite (0.550 µm spacing), was reached for the maximum percentage of niobium. Similar conclusions were shown by Mohrbacher and Zhai, who proposed that the decrease of the pearlite spacing was linked to a reduction in the diffusivity of carbon atoms due to the formation of Nb phases.[18] The dragging effect of niobium in solid solution prevents the diffusion of carbon atoms, therefore, only fine pearlite lamellar can be formed.[20] It is assumed that this drop of the pearlite lamellar spacing is related to changes in the mechanical properties.

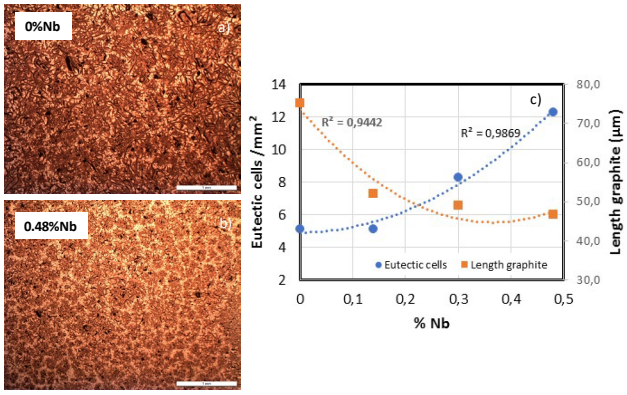

Figure 7. Effect of niobium content on eutectic cell structure: a) 0%Nb; b) 0.48%Nb, c) evolution in function of the additions of Nb.

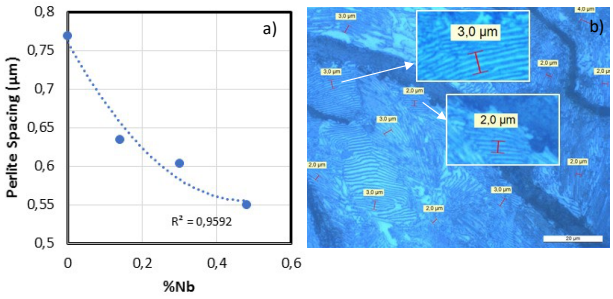

Figure 8. Effect of Nb alloy content on refinement of pearlite spacing: a) evolution of pearlite spacing, b) detail at 1000 magnifications of the measurements of this parameter at different positions.

INFLUENCE OF Nb ON MECHANICAL PROPERTIES

The effect of different niobium contents on the mechanical properties is shown in Table 4. According to these data, the addition of niobium implies a significant improvement both in tensile strength and in hardness (Figure 9). This tendency was also observed by other authors.[17,18] Maximum were reached in samples with 10mm of thickness and contents of 0.30%Nb (215HB and 196MPa). The hardening effect is related to the amount of niobium carbide phase formed. Additions of 0.48%Nb caused a slight loss of mechanical properties, probably by a high concentration of Nb particles in the matrix. The influence of niobium is less in thicker samples (lower cooling rate) leading to lower mechanical properties.

Table 4. Mechanical Properties for Samples with Two Different Thickness' for Several Nb Contents

%Nb	Tensile Strength (MPa)		Brinell Hardness (HB)	
	Thickness		Thickness	
	10mm	40mm	10mm	40mm
0	170	95	183	148
0.15	183	115	194	137
0.30	196	114	215	147
0.48	185	116	210	145

A detailed study of the microstructure was also carried out on these plates. Samples without niobium exhibit larger graphite, more kish graphite and lower number of eutectic cells than samples alloyed with niobium, verifying the conclusions obtained from the thermal analysis cups (Figure 9). These conclusions are more evident the smaller the thickness of the plates. As it was expected, the cooling rate affects directly the morphology of graphite and therefore to microstructure and mechanical properties.

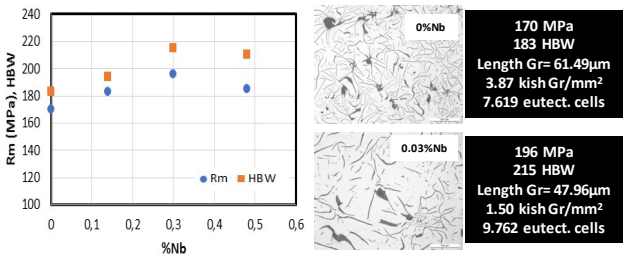

Figure 9. Evolution of mechanical properties and microstructure as a function of the %Nb for a plate with 10mm of thickness.

INFLUENCE OF Nb ON NUCLEATION POTENTIAL OF THE MELT

The nucleation of the graphite without any addition of niobium seems to occur around Mn-sulfides in a similar way to a conventional gray iron.[25,26] A close match between the lattice parameters of MnS and graphite was found by Hua Qu et al.[27] These complex Mn-S compounds, grow as a facetted cubic structure in a variety of shapes, and can appear embedded in the matrix without any visible contact with graphite, with a superficial contact between inclusion and graphite, or totally encapsulated by the graphite which seems to follow the shape of the non-metallic inclusion (Figure 10).[28]

Several AlO and (AlMg)O were found acting as nuclei for these sulfides. There is significant evidence in the literature about the key role played by Al in the flake graphite nucleation process,[29,30] with the formation of Al_2O_3 sites which act as excellent nucleants for (Mn,X)S compounds. These sulfides present a low crystallographic misfit with the graphite (δ=10.2)[31] versus the relatively large planar disregistry between Mn (111) and Al_2O_3 (111) (δ=28.8%).[32] This theory is endorsed by Riposan et al.[33] who proposed that graphite nucleation starts with the precipitation of complex oxides of Al, Si, Zr, Mg, Ti, followed by growth of complex (Mn,X) sulfides. According to Muhmond et al.,[34] there is a relationship between the final shape of Mn sulfides and the oxides that can appear in their core. In the absence of oxides in the melt, these particles grow with an irregular geometry consisting of small and large sizes according to the amount of sulfur present in the alloys.

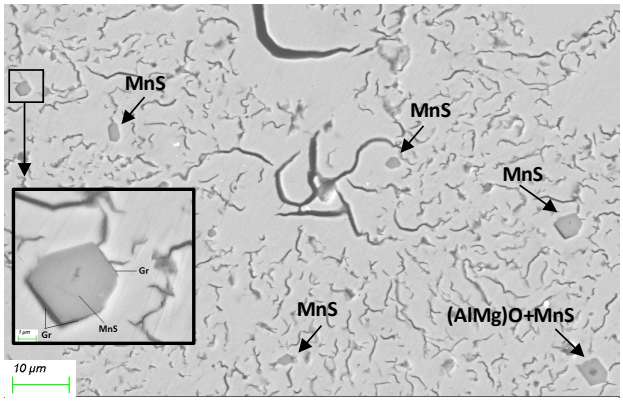

Figure 10. Nucleation of graphite on Mn sulfides for a hypereutectic gray iron without any addition of Nb.

An example of this kinetics of nucleation is illustrated in Figure 11 that shows graphite growing around a big inclusion following its polygonal shape. X-ray concentration graphs reveal that S and Mn show composition peaks at the same position. Then, Al, O, Zr and Mg also present coincidental maxima in the core of inclusion. Thus, this nucleus appears to be formed by a complex Al-Zr-Mg oxide surrounded by a big polygonal Mn sulfide, around which graphite grows, indicating a three-stage model for the nucleation of graphite.

The addition of niobium modifies the potential of nucleation of the melt. Mn sulfides continue to be the predominant inclusions, but some Nb compounds start to appear. Nb can combine with C, Ti and even Cr to form complex carbides type ,that can appear embedded in the matrix or in contact with graphite, acting as possible

nuclei for graphite. NbC will be formed in the liquid iron during the eutectic reaction. According to Sawamoto et al.,[35] Nb grows isomorphic as small cubes on Ti(C,N) nuclei. In most cases, Nb carbides are combined with Mn sulfides favoring the nucleation in different stages. The energy of formation of carbides is higher than sulfides so it assumed that they are formed later during the solidification process.[36,37,38]

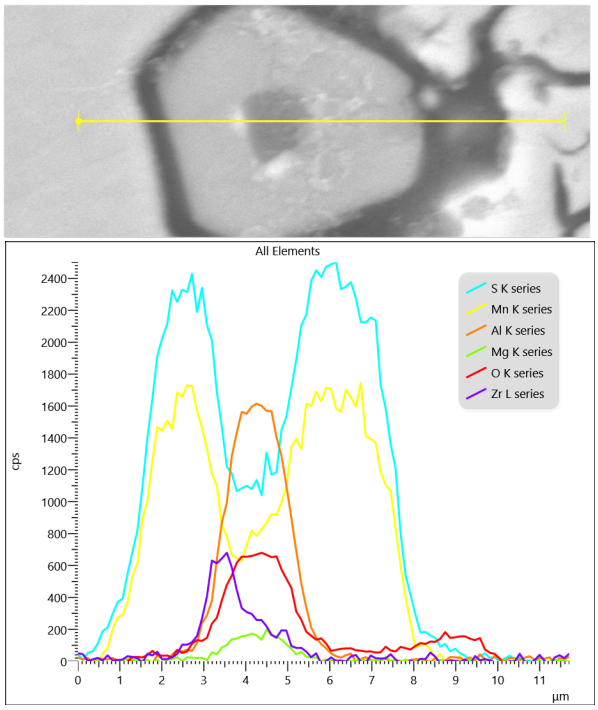

Figure 11. X-ray concentration graphs along a line through the core of a sectioned (Mn,X) particle.

No primary NbC precipitates were observed in the final solidified structure for the <0.005%Nb sample. For 0.15%Nb, niobium element preferentially partitions in NbC although its concentration in the matrix and as MC type carbides is very low. They are usually accompanied by Mn sulfides and it is necessary the analysis by spectrums to distinguish them (Figure 12a). For 0.30%Nb, the number of Nb compounds has increased significantly. They are apparently visible, precipitating as white cuboidal or polygonal particles which surround Mn sulfides in one or several directions (Figure 12b,c). These primary carbides, which exhibit a fine particle size and a homogeneous distribution, were also detected by other authors by similar contents of niobium.[17,18,39] They seem to be the responsible of the improvement of the mechanical properties. The huge affinity of niobium to carbon and the large number of Nb-rich phase particles would explain the refinement of the graphite. The quantification of the spectrums taken in Figure 12, reveals an increase of the %Nb in the precipitated inclusions, with the content of this alloy element in the melt (Table 5).

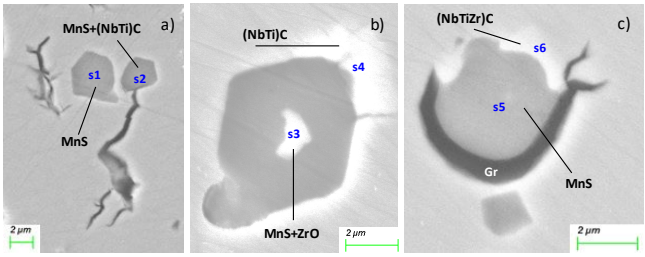

Figure 12. SEM micrographs of inclusions for melts with 0.15%Nb (a) and 0.30%Nb (b,c).

Table 5. Quantification of Spectrums (%weight) Taken in Inclusions in Figure 12.

Spec.	Mn	S	Nb	Fe	Ti	Zr	C
1	53.5	28.5	-	16.5	-	-	
2	48.4	26.3	4.1	17.8	1.5	-	1.8
3	34.3	20.0	-	9.4	-	28.9	2.7
4	9.1	5.4	64.7	7.3	7.1	-	5.5
5	56.1	30.3	2.3	6.0	0.4	-	4.5
6	1.7	1.2	57.9	24.3	7.2	2.9	4.2

For higher niobium contents (0.48%Nb) the number of small NbC precipitates growing into blocky and cuboidal shaped particles increased significantly. They can appear isolated or in contact with the graphite and alone or combined with Mn sulfides, acting as nuclei for graphite (Figure 13). In most cases, Nb compounds are enriched in other carburizers elements such as Ti or Cr.

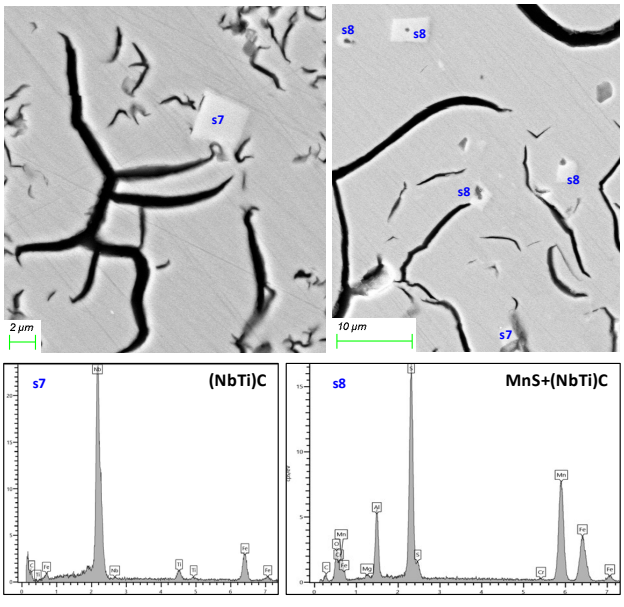

Figure 13. SEM micrographs of the quenched sample with 0.48%Nb, showing different polygonal Nb-carbides and their wavelength dispersive X-ray (WDX) spectrums.

In addition to these polygonal NbC carbides, small Nb-rich phases fine strip-like (including triangular, V and Y shaped) starts to appear (Figure 14). It is assumed that the combination of niobium and carbon happens in the late solidification stage, consuming the carbon in the final solidification zone. The formation of these small Chinese-script Nb-phases could be responsible of the slight loss of mechanical properties for 0.48%Nb (Table 4).

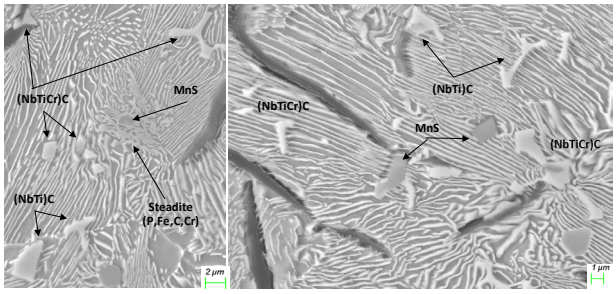

Figure 14. SEM micrographs of Nb-rich phases with Chinese -script shape dispersed in the matrix of the 0.48%Nb sample etched with Nital.

CONCLUSIONS

The influence of niobium additions on the microstructure of hypereutectic gray cast iron was investigated. A series of thermal analysis cups with percentages of Nb from 0% to 0.48%, treated with inoculant containing Zr and Mn, were produced.

A significant effect was observed during the solidification process. Parameters such as liquidus temperature, eutectic minimum temperature and recalescence decreased when the content of niobium increased.

Addition of Nb changed the final microstructure of the alloy, refining the eutectic cells and the graphite, decreasing the cell size, leading to shorter and finer the graphite flakes. The formation of spider-shape graphite, known as kish graphite, is also minimized. The spacing of pearlite lamellar is reduced considerably. An improvement of the mechanical properties was found, reaching the maximum for a content of 0.30%Nb.

Niobium participates actively in the nucleation process. It forms primary MC-type carbides, exhibiting a fine particle size and homogeneous distribution. The number on Nb particles increases with the content of niobium in the melt. They appear in the matrix or acting as nuclei for graphite usually accompanied by Mn sulfides. These Nb-phases can adopt different shapes, cuboidal, triangular, blocky or Chinese-script depending on the content of niobium. The formation of these niobium precipitates seems to be related to the amelioration of the mechanical properties.

ACKNOWLEDGMENTS

This work was supported by Diputación Foral de Bizkaia, Spain.

REFERENCES

1. EL-Sawy, E.E.T., EL-Hebeary, M.R., EL-Mahallawi, I.S.E., “Effect of Manganese, Silicon and Chromium Additions on Microstructure and Wear Characteristics of Gray Cast Iron for Sugar Industries Applications,” *Wear*, 390-391, 113-124 (November 2017).
2. Riposan, I., Chisamera, M., Stan, S., White, D., “Complex (Mn,X)S Compounds – Major Sites for Graphite Nucleation in Grey Cast Iron,” China Foundry, 6 (4), 352-358 (November 2009).
3. McGrath, M.C., Richards, V., Anish, T.V., “Effects of Nitrogen, Titanium and Aluminum on Grey Cast Iron Microstructure,” *AFS Transactions* (2009).
4. Stefanescu, D.M., Alonso, G., Larrañaga, P., Suarez, R., “On the Stable Eutectic Solidification of Iron-Carbon-Silicon Alloys,” Acta Materiala, 103, 103-114 (2016).
5. Alonso, G., Stefanescu, D.M., Larrañaga, P., De la Fuente, E., Suarez, R., “On the Nucleation of Graphite in Lamellar Graphite Cast Iron,” *AFS Transactions*, 124, 205-213 (2016).
6. Azzough, M.O., Boutarek, N., Drif, R., Madaoui, N., Boulgheb, K., “Metallurgical, Mechanical and Electrochemical Behaviour Study of the Lamellar Gray Cast Iron Treated with Vanadium,” *5th International Science Congress & Exhibition APMAS2015*, Oludeniz, Turkey, 548-551 (April 2015).
7. Atanda, P., Okeowo, A., “Microstructural Study of Heat Treated Chromium Alloyed Grey Cast Iron,” *J. Minerals Mater. Charact. Eng*., 9 (3), 263-274 (2010).
8. Awad, E.G.A.M., Abdulsalam, K., “Enhancement of the Gray Cast Iron Properties by Adding Chromium Element,” *Key Engineering Materials*, 753, 218-221 (2017).
9. Kus, R., Akgul, B., “Experimental Investigation on the Effect of Tin (Sn) in Gray Cast Iron to Impact Strength Hardness and Microstructure,” *International Journal of Mechanical and Production Engineering*, 6 (12), 39-42 (December 2018).
10. Bates, C.E., “Effects of Alloy Elements on the Strength and Microstructure of Gray Cast Iron,” *AFS Trans*., 923-946 (1984).
11. Chen, Y., Xue, Z., Song, S., Cromarty, R., Zhou, X., “Evolution of the Microstructure and High Temperature Tensile Strength of Gray Cast Iron HT250: The Role of Molybdenum,” *Materials Science & Engineering A*, 863 (2023).

12. Ankamma, K., "Effect of Trace Elements (Boron and Lead) on the Properties of Gray Cast Iron," *J. Inst. Eng. India Ser. D*, 95 (1), 19-26 (2014).
13. Fallon, M.J., The Effect of Some Trace Elements in Cast Iron," *Indian Foundry J*., 26 (6), 1 (1980).
14. Naro, R.L., Wallace, J.F., "Minor Elements in Gray Cast Iron," *AFS Transactions*, 88, 229 (1980).
15. Loper C.R. Jr, Park, J., "On the Mechanism of the Formation of Widmanstätten Graphite in Flake Graphite Cast Irons*," Metals and Materials International*, 9 (4), 327-336 (2003).
16. Alonso, G., Gallastegui, I., Suarez, R., "Mechanisms of Formation of Degenerated Graphite in Lamellar Graphite Cast Iron," 74th World Foundry Congress, Busan, Republic of Korea (October 2022).
17. Deceveli, A.O., Yakut, R., "The Effect of Nb Supplement on Material Characteristics of Iron with Lamellar Graphite," *Advances in Materials Science and Engineering* (January 2014).
18. Mohrbacher, H., Zhai, Q., "Niobium Alloying in Grey Cast Iron for Vehicle Brake Discs," *Materials Science and Technology (MS&T)*, 434-445 (October 2011).
19. Zhou, W., Zhu, H., Zheng, D., Zheng, H., Hua, Q. Zhai, Q., "Nb Alloying Effect in High Carbon Equivalent Gray Cast Iron," *China Foundry*, 1 (8), 36-40 (2011).
20. Pan, S., Zeng, F., Su, N., Xian, Z. "The Effect of Niobium Addition on the Microstructure and Properties of Cast Iron used in Cylinder Head," *Journal of Materials Research and Technology*, 9 (2), 1509-1518 (2020).
21. Castro, M.J., Lacaze, J., Regordosa, A., Sertucha, J., Del Campo, R., "Revisiting Thermal Analysis of Hypereutectic Spheroidal Graphite Cast Irons," *Metallurgical and Materials Transactions A*, 51A, 6373-6385 (December 2020).
22. Liu, S, Loper, C.R. Jr., "The Formation of Kish Graphite," *Carbon*, 29, 547-555 (1991).
23. López, M, Massone, J.M., Boeri, R.E., "Evolution of the Macrostructure of Gray Cast Iron from Eutectic to Hypereutectic Composition," *Materials Science Forum*, 925, 110-117 (2018).
24. Alonso, G., Stefanescu, D.M., Larrañaga, P., Sertucha, J., Suarez, R. "Gray Cast Iron with High Austenite-to-Eutectic Ratio Part I – Calculation and Experimental Evaluation of the Fraction of Primary Austenite in Cast Iron," *AFS Transactions,* 120, 329-335 (2012).
25. Chisamera, M., Riposan, I., Barstow, M., *AFS International Inoculation Conference*, Rosemont, II, USA, paper 3 (1998).
26. Skaland, T., Grong, Ø., Grong, T., "A Model for the Graphite Formation in Ductile Cast Iron: Part II. Solid State Transformation Reactions," *Metallurgical Transactions A,* 24, 2347-2353 (October 1993).
27. Qu, H., Weidong, L., *Adv. Mater. Res*., 299-300, 576-579 (2011).
28. Alonso, G., Stefanescu, D.M., Larrañaga, P., De la Fuente, E., Suarez, R., "On the Nucleation of Graphite in Lamellar Graphite Cast Iron," *AFS Transactions*, 124, 205-213 (2016).
29. Riposan, I., Chisamera, M., Stan, S., Skaland, T.,"A New Approach to Graphite Nucleation Mechanism in Gray Irons," *Proceedings of the AFS Cast Iron Inoculation Conference*, Schaumburg, Illinois (September 2005).
30. Riposan, I., Chisamera, M., Stan, S., Skaland, T, Onsoien, M.I., "Analyses of Possible Nucleation Sites in Ca/Sr Over-Inoculated Gray Irons," *AFS Transactions*, 109, 1151-1162 (2001).
31. Wendog, X., Li, Y., "Pretreatments of Gray Cast Iron with Different Inoculants," *Journal of Alloys and Compounds*, 689, 408-415 (2016).
32. Wakoh, M., Sawai, T., Mizoguchi, S., *ISIJ Int*., 36, 8, 1014-1021 (1996).
33. Riposan, I., Chisamera, M., Stan, S., Hartung, C., White, D., in the *Carl Loper Cast Iron Symposium*, Madison, WI, USA, 191-200 (2009).
34. Muhmond, H.M., Fredriksson, H., "Relationship Between Inoculants and the Morphologies of MnS and Graphite in Gray Cast Iron," *Metallurgical and Materials Transactions B*, 44, 283-298 (2013).
35. Sawamoto, A., Ogi, K., Matsuda, K., *AFS Transactions*, 403, 72-86 (1986).
36. Ellingham, H., *Transactions and Communications. J. Soc. Chem. Ind*., (1944).
37. Alonso, G., Bravo, B., Stefanescu, D.M., Suarez, R., "Evolution of the Metallurgical Quality of Spheroidal Graphite Iron during the Thermal Cycle of the Melt: Furnace – Ladle – Heating/Pouring Unit," AFS Proceedings of the 127st Metalcasting Congress, Ohio (25-27 April 2023).
38. Alonso, G., Stefanescu, D.M., Bravo, B., Suarez, R., "Graphite Spheroids – The Place Where They are Born" *Keith Millis Symposium*, Atlanta, USA (October 2023).
39. Mohrbacher, M., "The Beneficial Effect of Niobium Alloying in Gray Cast Iron – Fundamentals and Applications," CBMM, Niobium Nb (2015).